Anti-Cancer Agents in Medicinal Chemistry, 2022, *22*, 2340-2351

RESEARCH ARTICLE

New Synthetic Sulfonamide Chalcone Induced Cell Cycle Arrest and Cell Death in Colorectal Adenocarcinoma Metastatic Cells (SW-620)

Andréa Felinto Moura[1,*], Mirian Rita Carrilho de Castro[2], Raquel Ferreira Naves[2,3], Ana Jérsia Araújo[4], Maria Claudia Luciano dos Santos[1], José Delano Barreto Marinho Filho[4], Caridad Noda-Perez[2], Felipe Terra Martins[2], Claudia do Ó Pessoa[1] and Manoel Odorico Moraes Filho[1]

[1]*Departamento de Fisiologia e Farmacologia, Núcleo de Pesquisa e Desenvolvimento de Medicamentos - NPDM, Universidade Federal do Ceará, Fortaleza, CE, Brazil;* [2]*Instituto de Química, Universidade Federal de Goiás, Goiânia, GO, Brazil;* [3]*Instituto Federal de Goiás, Campus Inhumas, Inhumas, GO, Brazil;* [4]*Departamento de Biotecnologia, Universidade Federal do Delta do Parnaíba, Parnaíba, PI, Brazil*

Abstract: ***Background*:** New chalcones have been developed from the insertion of organic groups, among them sulfonamides, presenting varied biological activity.

***Objective*:** The aim of this work was to determine the antitumor potential of a new synthetic sulfonamide chalcone (SSC185) against a colorectal metastatic lymph node-derived colorectal cancer cell line (SW-620).

***Methods*:** Synthesis and characterization, including crystallography, of SSC185 were performed. SSC185 showed a selective cytotoxic effect against colorectal cancer cell lines. Therefore, the cytotoxic effect of SSC185 against SW-620 was further investigated. We used optical and fluorescence microscopy, flow cytometry and Western blot to determine the antitumor effects of SSC185.

***Results*:** SSC185 induced cytotoxicity in SW-620 cells in a time and concentration-dependent manner. Cell cycle progression was disrupted, with increased G2/M cell number and consequent cell death, with morphological alterations associated with apoptosis and necrosis. Cell death was associated with the activation and cleavage of PARP, and with reduced expression of the pro-apoptotic Bax protein and caspase 8, depending on the SSC185 concentration tested. Expression of the necroptosis pathway proteins RIP and MLKL was also reduced. These proteins are phosphorylated during the process of necroptosis.

***Conclusion*:** We suggest that the mechanism involved in the cytotoxic effect of SSC185 against SW-620 *in vitro* may be related to the induction of cell cycle arrest in the G2/M phase and cell death by apoptosis or necroptosis, depending on the concentration used.

ARTICLE HISTORY

Received: April 24, 2021
Revised: August 26, 2021
Accepted: November 01, 2021

DOI:
10.2174/1871520621666211213092121

Keywords: Synthesis, cytotoxicity, cell death, apoptosis, necroptosis, cancer.

1. INTRODUCTION

Cancer is a complex disease involving the disordered growth of abnormal cells with invasive potential [1, 2]. The disordered growth of cells in cancer is a result of self-sufficiency in signaling growth factors and insensitivity to growth inhibitors, providing a selective proliferative advantage to malignant cells. In addition, malignant cells are better at adapting to stressful conditions, often evading programmed cell death and utilizing the immune system to their advantage. Thereby, malignant cells have unlimited replicative potential, being able to reprogram their energy metabolism, invade and metastasize and promote angiogenesis, which results in their immortalization [3, 4]. Thus, it is important that new therapeutic strategies are developed to eliminate tumor mass (whilst protecting normal cells and minimizing patient discomfort) with greater effectiveness.

Chalcones are precursors of flavonoids and isoflavonoids, present in many plants and bacteria, with broad biological activity including antitumor effect. These molecules are easily obtained from the Claisen-Schmidt condensation reaction, allowing the synthesis of chalcone derivatives. A promising strategy being used to develop new chalcones is the addition of organic groups, such as aromatic ring substituents [5]. Among the possible substituents, sulfonamides are an important structural class of drug molecule, with biological activities such as anticancer, antibacterial, and antimalarial. The anticancer effects of chalcones can be enhanced by molecular hybridization to different compounds with interesting pharmacological properties [6].

Some biological activities of sulfonamide chalcones have been described, such as antifilarial [7], antimalarial [8], antibacterial [9] and anticancer [10-14], as well as α-glucosidase inhibitor [15], β-secretase and acetylcholinesterase inhibitor [16], carbonic anhydrase inhibitor [17-19] and ecto-5'-nucleotidase and intestinal alkaline phosphatase inhibitor [20]. However, the anticancer mechanism of these molecules is yet to be explored. Despite the significance of the antitumor potential of sulfonamide chalcones, few studies describe the possible pathways related to this effect. In a recently published study, sulfonamide chalcones with an antitumor effect *in vitro* that were submitted to structure-based pharmacophoric screening *in silico*, showed a strong potential activity as mitogen activated

*Address correspondence to this author at the Departamento de Fisiologia e Farmacologia, Núcleo de Pesquisa e Desenvolvimento de Medicamentos - NPDM, Universidade Federal do Ceará, Rua Cel. Nunes de Melo 1000, Fortaleza 60431-270, CE, Brazil; Tel/Fax: +5586999656292;
E-mail: andreafmoura@gmail.com

1875-5992/22 $65.00+.00

protein kinase 10 (JKN3) inhibitors [21]. However, further studies are needed to confirm these findings. In fact, since both sulfonamide and chalcone motifs exhibit antitumor activities, their conjugate compounds are also promising anticancer candidates [22-24].

The incidence of cancer increases every year, demonstrating the relevance of conducting research on cancer treatment in its various modalities. Thus, this work aimed to study the antitumor potential of a new synthetic sulfonamide chalcone (SSC185) by *in vitro* assays, evaluating the biochemical and molecular markers of cell death in colorectal cancer-derived metastatic cells (SW-620).

2. MATERIALS AND METHODS

2.1. Synthesis and Physicochemical Characterization of SSC185

A new synthetic sulfonamide chalcone *μ*-(2,5-dichloro-*N*-{4-[(3*E*)-4-(3-nitrophenyl) buta-1,3-dien-2-yl] phenyl} benzene sulfonamide), identified as SSC185, was synthesized by Claisen-Schmidt condensation. In a round-bottom flask, 1.0 mmol of N-(4-acetylphenyl)-2,5-dichlorobenzenesulfonamide and 2.0 mmol of 3-nitro-benzaldehyde in 10 mL of ethanol was added. KOH solution (50% w/w as a function of N-(4-acethylphenyl)-2,5-dichloroben zenesulfonamide) was added to the reaction mixture as a catalyst. The reaction was continuously stirred at room temperature and monitored by thin layer chromatography (TLC). After 24 h, ice water was added to the reaction mixture and the precipitate formed was filtered and dried. Recrystallization was achieved using a methanol-acetone mixture, which yielded a potassium salt monohydrate. The melting points were measured on Karl Kolb apparatus (Frankfurt, Germany). ^{1}H and ^{13}C NMR spectra were recorded on a Bruker Avance III 500 (500.15/125.77 MHz for $^{1}H/^{13}C$) spectrometer using deuterated DMSO with TMS (Bruker Optik GmbH, Ettlingen, Germany). Infrared (IR) spectra were performed on a Bruker IFS-55 FT spectrometer (Bruker Optik GmbH, Leipzig, Germany). Mass spectra analysis was performed using a micrOTOF-Q III mass spectrometer (Bruker Daltonics, Bremen, Germany). The ^{1}H NMR, ^{13}C NMR and mass spectra are included in the Supplementary Information.

Yellow crystalline solid, 242-245°C, yield 99%. ^{1}H (DMSO-d_6, 500 MHz): δ 8.71 (dd, *J*=1.83 Hz and 2.44 Hz, H-2, 1H), 8.29 (ddd, *J*=1.22 Hz, 1.83 Hz and 7.93 Hz, H-4, 1H), 8.23 (ddd, *J*=1.22 Hz, 2.44 Hz and 8.24 Hz, H-6, 1H), 8.09 (d, *J*=15.58 Hz, H-*β*), 7.97 (dd, *J*=1.53 Hz and 1.22 Hz, H-12', 1H), 7.90 (d, *J*=8.85 Hz, H-3' and H-1', 2H), 7.71 (dd, *J*=7.93 Hz and 8.24 Hz, H-5, 1H), 7.70 (d, *J*=15.58 Hz, H-α, 1H), 7.47-7.46 (m, H-9' and H-10', 2H), 6.86 (d, *J*=8.85 Hz, H-4' and H-6', 2H). ^{13}C (DMSO-d_6, 500 MHz): δ 186.42 (C=O), 156.93 (C-5'), 148.91 (C-3), 146.17 (C-7'), 139.27 (C-*β*), 137.65 (C-1), 135.20 (C-4), 133.33 (C-10'), 131.39 (C-11'), 131.16 (C-9'), 130.72 (C-5), 130.67 (C-3' and C-1'), 130.16 (C-8'), 129.79 (C-12'), 126.45 (C-2'), 125.92 (C-*α*), 124.52 (C-6), 123.17 (C-2) and 120.36 (C-4' and C-6'). FTIR (KBr, cm^{-1}) 3085 (N-H), 1589 (Ar-CO-C=C-Ar), 1648 (C=O), 1348 (S=O), 1533-1448 (C=C-Ar), 1172 (Ar-Cl). HRMS calculated for $C_{21}H_{14}Cl_2N_2O_5S$ 477.3173, found 477.9877.

2.2. Crystallographic Methodology

The selected single crystal of SSC185 was mounted and aligned on a κ-goniostat before exposition to X-ray beam from Mo anode (Kα, λ = 0.71073 Å) using a Bruker-AXS Kappa Duo diffractometer with an APEX II CCD detector. Bruker programs SAINT and SADABS [25] were used for cell refinement and data indexing, integration, and reduction. Structure solution and refinements were performed using the programs SIR2004 [26] and SHELXL-2018 [27], respectively, both within WinGX [27]. Structure analysis and artwork preparation were performed using MERCURY [28] and ORTEP-3 [29] software. Non-hydrogen and hydrogen atoms were refined anisotropically and isotropically, respectively. All CH hydrogens were added to their corresponding carbons following a riding model with fixed bond lengths and angles. Water hydrogens were also fixed during refinements, even though they were first localized in the difference Fourier map and accordingly checked for their intermolecular directionality. Hydrogens had their isotropic atomic displacement parameters set to 1.2 Uiso of the corresponding carbon, except for the hydrogen atoms of water molecules, for which this value was increased to 1.5. The complete X-ray diffraction dataset is available at https://www.ccdc.cam.ac.uk/, under CCDC number 1992701, and a summary of data collection and processing is provided in the (Table **S1**, Supplementary Material).

2.3. Cell Cultures

Human and murine cell lines were used for cytotoxicity assays. PC-3 (prostate), HCT-116 (colon), SF-295 (brain), NCI-H460 (lung), SW-620 (metastatic colon), HEP-G2 (liver), MCF-7 (breast), HL-60 (promyelocytic leukemia) and L-929 (fibroblast) non-tumor cell lines were provided by the National Cancer Institute (Bethesda, MD, USA). Cell lines were maintained as a monolayer culture in RPMI 1640 (Gibco) or DMEM (Gibco) medium, supplemented with 10% fetal bovine serum and 2 mM glutamine, 100 U/mL penicillin, and 100 μg/mL streptomycin at 37°C with 5% CO_2. Peripheral blood mononuclear cells (PBMC) were also tested. PBMC were obtained by primary culture from heparinized blood from healthy and non-smoking donors, using the method described by Moura and collaborators [30].

2.4. Cytotoxicity Assay

The cytotoxic effect of SSC185 against tumor and non-tumor cell lines was evaluated by MTT assay. This assay is a quantitative colorimetric method that allows quantification of cell viability by the reduction of the tetrazolium 3-(4,5-dimethyl-2-thiazole)-2,5-diphenyl-bromide (MTT) salt by metabolically active cells with a consequent formation of formazan crystals [31]. Cells were plated in 96-wells plates and treated with SSC185 concentrations ranging from 0.4 to 52.4 μM, or with DMSO (vehicle). Doxorubicin was used as a positive control. At the end of the incubation period, the plates were centrifuged, and the supernatant was removed and replaced with fresh medium containing MTT (0.5 mg/mL). The plates were incubated for 3 h, and the MTT formazan product was dissolved in DMSO. Cell viability was quantified using a microplate reader (Spectra Count, Packard, Ontario, Canada) at 595 nm and growth inhibition was estimated.

To investigate the influence of N-acetyl-cysteine (NAC) on the cytotoxicity of SSC185, SW-620 cells were pre-treated with NAC (4 mM) for two hours. After the incubation period, the medium containing NAC was removed and cells were treated with SSC185, or DMSO (vehicle) or Menadione (positive control) in concentrations ranging from 0.2 to 50 μM. The plates were then incubated again for 48 h. A no pre-treatment control plate was concurrently assayed to ensure that NAC did not alter cell viability. Cell viability was assessed by the MTT assay, as previously described.

2.5. Monitoring of Cell Proliferation by Real-Time Cell Analysis

Inhibition of SW-620 cell growth during treatment with SSC185 was monitored using the xCELLigence real-time cell analysis (RTCA) system (ACEA Biosciences). SW-620 cells were seeded (5 x 10^3 cells/mL) in 16-well plates (E-plate 16, Roche, Mannheim, Germany). Cell adherence, disposition and proliferation were monitored every 30 minutes by the RTCA-DP (dual purpose) instrument. Approximately 24 h after plating, the SW-620 cells were treated for 72 h with SSC185 dissolved in a culture medium. DMSO (vehicle) was used as a negative control and doxorubicin (0.5 μM) was used as a positive control. The SSC185 compound was tested at concentrations of 2.5; 5; 7.5; 10 and 15 μM, which

were determined from the results of the MTT assay. The average baseline cell index and percent reduction of baseline cell index for SSC185-treated cells compared to control cells were calculated for each incubation period analyzed (24 h, 48 h and 72 h).

2.6. Morphological Analysis

Morphological changes of SW-620 cells treated with SSC185 were analyzed by optical microscope. Cells were plated and treated with SSC185 at 10 and 15 μM (concentrations with better inhibitory activity) over 24 and 48 h. DMSO (vehicle) was used as a negative control and doxorubicin (0.5 μM) was used as a positive control. After incubation, cells were fixed and counterstained using the Fast-Panoptic kit (Laborclin Ltd, Paraná, Brazil). The cells were analyzed by light microscopy (Olympus, Tokyo, Japan) at 200× magnification.

2.7. Flow Cytometry Analysis

For flow cytometry analysis, SW-620 cells were plated and treated with SSC185 at concentrations of 10 and 15 μM, or with DMSO (vehicle) for 24 h. Doxorubicin (0.5 μM) was used as a positive control. Fluorescence was measured using a Guava easyCyte 6-2L flow cytometer (Merck Millipore). At least three independent experiments were performed in triplicate and ten thousand events were evaluated per experiment.

2.7.1. Cell Number Counting and Membrane Integrity Analysis

After incubation, treated and untreated SW-620 cells were incubated with propidium iodide solution (50 μg/mL) in the dark for 5 minutes. Fluorescence was measured by flow cytometry. Data were obtained on the number of cells, morphology (forward and side scatter of the light, which corresponds to the size and relative granularity of the cells, respectively) and cell membrane integrity [32].

2.7.2. Cell Cycle and DNA Fragmentation Analysis

Cell cycle analysis of SSC185-treated SW-620 cells was performed by flow cytometry. After incubation, the plasma membrane of the treated and untreated cells was permeabilized using a lysis solution (0.1% sodium citrate, 0.1% Triton X-100), and the DNA content was stained with propidium iodide (50 μg/mL) in PBS. After incubating in the dark for 30 minutes, the samples were analyzed on the flow cytometer. Fluorescence was measured and cell cycle was analyzed using the program ModFit LT version 3.1 for Win32, which was also used to quantify DNA fragmentation by the Sub-G1 (debris) percentage.

2.7.3. Mitochondrial Transmembrane Potential Analysis

A 200 μL aliquot of treated or untreated cell suspension was centrifuged and the pellet was resuspended in 200 μL of rhodamine 123 solution (1 μg/mL). After incubation (5% CO_2 at 37°C) in the dark for 15 minutes, the samples were centrifuged at 2000 rpm for 5 minutes, the supernatant was removed, and the cells were resuspended in 200 μL of PBS and incubated at room temperature in the dark for another 30 minutes. The samples were then analyzed by flow cytometry [33].

2.8. Fluorescence Microscopy Analysis

To detect and quantify the cell death pattern induced by SSC185, SW-620 cells were stained with acridine orange and ethidium bromide and analyzed by fluorescence microscopy. SW-620 cells were plated and treated with SSC185 at concentrations of 10 and 15 μM, or with DMSO (vehicle) for 24 h. Doxorubicin (0.5 μM) was used as a positive control. After the incubation period, a 50 μL aliquot of cell suspension was stained with 1 μL of a solution containing 8 μL of PBS, 2 μL of acridine orange (100 μg/mL) and 10 μL of ethidium bromide (20 μg/mL). Three hundred cells were classified and counted under a fluorescence microscope. All experiments were performed in triplicate.

2.9. Western Blot

Untreated and treated SW-620 cells with SSC185 for 24 h were lysed in cold radio-immunoprecipitation assay buffer (RIPA - Millipore) supplemented with PMSF (1:100 v/v - Sigma), sodium orthovanadate (1:100 v/v - Sigma) and protease inhibitor cocktail (1:100 v/v - Sigma).

Protein concentrations were estimated using the DC Protein Assay kit (BioRad Laboratories). 30 μg of total protein from each sample was loaded into the stacking gel, and separated by 12.5% SDS-polyacrylamide gel electrophoresis, and then transferred onto polyvinylidene difluoride (PVDF) membranes (Millipore). The membranes were blocked with 5% (v/v) skim milk in TBS buffer containing 0.1% Tween-20 for 1 h and then incubated with the primary antibody for detection of cell signaling (Cyclin B1, pChk1, pChk2, PARP, Bax, Caspase-8, RIP, MLKL and β-actin) (1:1000 v/v - *Cell Signaling Technology*®) overnight at 4°C. After washing, the membranes were incubated with horseradish peroxidase-conjugated anti-mouse or anti-rabbit IgG antibodies (1:2000 v/v - Cell Signaling Technology®). The membranes were visualized using a chemiluminescent kit (Clarity and Clarity Max Western ECL Blotting Substrates, BioRad) and detected using ImageQuant300 (GE Healthcare Life Sciences) according to the manufacturer's instructions. The images were quantified using the Image J program [34].

2.10. Statistical Analysis

All analyses were carried out using GraphPad Prism (Intuitive Software for Science, San Diego, California, USA). The IC_{50} values and their 95% confidence intervals (CI 95%) were obtained by non-linear regression. Data analysis was based on the mean ± S.E.M of at least three independent experiments. Differences between the experimental groups were compared by one-way analysis of variance (ANOVA) followed by Tukey's test, with a significance level of 5% (p <0.05).

3. RESULTS AND DISCUSSION

3.1. Physicochemical Characterization and Crystallographic Analysis

The results of ^{1}H and ^{13}C NMR and FTIR spectra confirmed that the synthesized compound is a sulfonamide chalcone, identified as SSC185, which was obtained with high purity (Fig. **1**). The NMR spectra are available in the Supplementary Information.

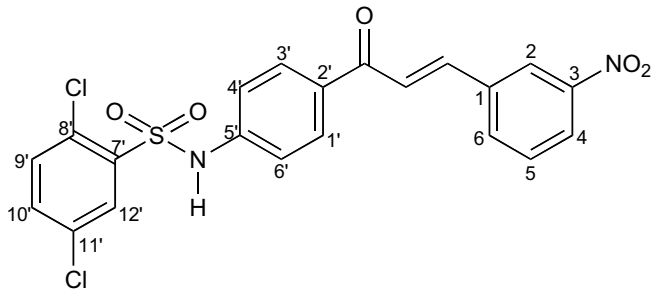

Fig. (1). Structure of μ-(2,5-dichloro-*N*-{4-[(3*E*)-4-(3-nitrophenyl)buta-1,3-dien-2-yl] phenyl}benzene sulfonamide), identified as SSC185.

The crystal structure of SSC185 was elucidated by single-crystal X-ray diffraction technique. The ORTEP-3 representation of its experimental molecular backbone in the solid state is shown in

Fig. (**2**), and all information related to the collection, treatment and refinement of the crystal structures can be found in the (Table **S1**).

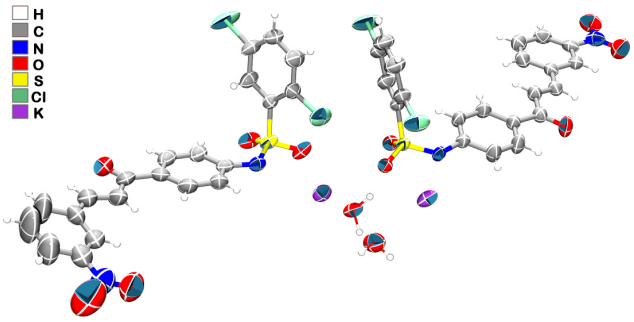

Fig. (2). Asymmetric unit of the potassium salt monohydrate of SSC185. Non-hydrogen atoms are represented as 50% probability ellipsoids following a Fig. (1) labelling (NMR assignments), while hydrogens are shown as arbitrary radius spheres. (*A higher resolution / colour version of this figure is available in the electronic copy of the article*).

SSC185 crystallized in the triclinic centrosymmetric space group P-1, as a potassium salt monohydrate. Unlike all other related chalcone-sulfonamide hybrids [35-37], SSC185 crystallizes as potassium salt in its deprotonated form. In contrast, all others crystallized in their neutral form under the same alkaline conditions. This reveals a higher acidity of SSC185 when compared to its related compounds. In fact, here, we have chosen 3-nitro and 2,5-dichloro substituents to increase the acidity of the sulfonamide group due to their electron withdrawing abilities. Electron deficiency would be more pronounced on the sulfonamide group with ortho and para substitutions at the central benzene ring. However, ortho analogues have a propensity either to assemble intramolecular hydrogen bonding between sulfonamide and carbonyl groups or for intramolecular cyclization [35]. Therefore, we have prepared a para-substituted analogue, which has an increased tendency to lose its NH hydrogen and hold a negative charge, putatively playing a key role in its striking cytotoxicity. For instance, its deprotonated sulfonamide group can interact electrostatically with cellular macromolecules as a hydrogen bonding acceptor from amino acid residues bearing OH, NH, NH+ or SH groups, which is impossible for its non-ionized parent compounds with the protonated NH moiety.

However, the asymmetric unit was made up of two anionic molecules of SSC185, which were present with deprotonated sulfonamide groups, two potassium counterions and two crystallizing water molecules (Fig. **2**). The two crystallographically independent molecules of SSC185 were labeled A and B and are not similar conformationally. These are classical conformers differing profoundly for rotations on two bond axes, namely, N2-C5' and C1-C15 (Fig. **3**). There is a ca. 180° twist on N2-C5', as can be viewed, for instance, on the S1-N2-C5'-C6' torsion values for conformers A [166.9(3)°] and B [-0.8(5)°]. As a consequence of this rotation, the nitrogen lone pairs are pointed towards the same side of the carbonyl oxygen in molecule B, while they face opposite sides in molecule A.

In both molecules, the 2,5-dichlorobenzene mean plane is almost perpendicular to the chalcone average plane crossing through the carbons of rings B and C and propenone non-hydrogen atoms (Fig. **3**), as can be viewed by the angle between these aforementioned planes [81.61(11)° in molecule A and 74.02(7)° in B]. However, the halogenated ring has an opposite orientation relative to the chalcone basis in the two conformers, also resulting from the ca. 180° rotation on N2-C5' (Fig. **3**). The other rotation, on C1-C15, deviates slightly from 180°, as can be noted in the C14-C15-C1-C2 torsion values [11.8(10)° in A and 172.3(4)° in B] (Fig. **3**). Moreover, this rotation is responsible for two phenomena in the molecular backbone of SSC185. First, nitro groups are pointed towards opposite sides relative to the carbonyl oxygen, following the same pattern of lone nitrogen pairs in the conformers A and B. Second, the chalcone core of molecule A is more bent than that of molecule B (the root-mean-square deviation for the non-hydrogen atoms of the above defined chalcone plane is 0.225 Å in molecule A, against a lower value, and therefore higher planarity, of 0.0883 Å in molecule B). In the solid state, potassium ions are mainly surrounded by sulfonamide atoms and water oxygens, even though chlorine atoms and one nitro oxygen are also bonded to K+ ions. Their coordination environment draws an 8-vertices polyhedron with six oxygens, one chlorine and one nitrogen (Fig. **4**).

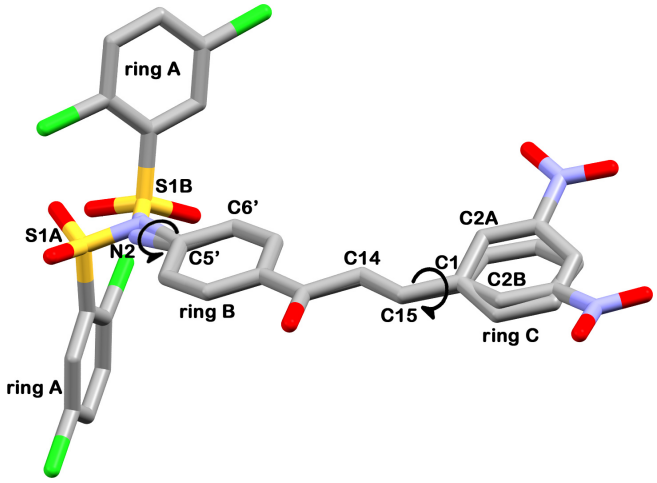

Fig. (3). Molecular overlay through propenone moiety for conformers A and B present in the potassium salt monohydrate of SSC185. Round arrows indicate ca. 180° rotations converting a conformation into another one. Ring labelling scheme is shown, as well as key atom labels are also depicted (labels ending with either A or B refer to the corresponding molecule, while superimposed atoms in the drawing had their labels shown only with characters common to both conformers, *i.e.*, omitting A or B). (*A higher resolution / colour version of this figure is available in the electronic copy of the article*).

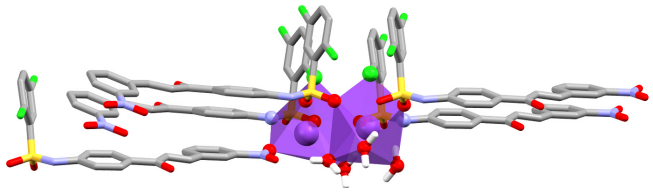

Fig. (4). Coordination polyhedron of the two crystallographically independent potassium ions. Vertex atoms and potassium ions were outlined as spheres to highlight the polyhedral enclosing. (*A higher resolution / colour version of this figure is available in the electronic copy of the article*).

3.2. Cytotoxicity Effect of SSC185 Against Tumor and Non-Tumor Cell Lines

Molecules containing sulfonamide and chalcone moieties may lead to new hybrid architectures with improved biological profiles [6, 12, 14, 24]. Recent studies have reported the chemical synthesis of new sulfonamide chalcones and their antitumor potential. The antitumor effect of these molecules *in vitro* has been described in some tumor cell lines, such as, MCF-7 (breast cancer) [6], K562 (leukemia) and LOX IMVI (melanoma) [10], SF-295 (glioblastoma), PC-3 (prostate cancer) and HCT-116 (colorectal cancer) [18],

and HEPG2 (liver cancer) [24]. However, no studies have described the mechanism of cell death involved in the antitumor effect of sulfonamide chalcones.

The cytotoxic effect of SSC185 against tumor and non-tumor cell lines was evaluated by MTT assay after 72 h of incubation (Table **1**). SSC185 showed antiproliferative potential against all tumor and non-tumor cell lines tested, with lower IC_{50} values for the colorectal cancer cell lines HCT-116 (5.59 μM) and SW-620 (6.27 μM) and leukemia cell line HL-60 (8.46 μM), while for the other tumor cell lines (MCF-7 and PC-3) the IC_{50} value was 19.76 and 29.52 μM respectively. The IC_{50} value of SSC185 against non-tumor cell lines L-929 and PBMC was 24.10 and 22.54 μM, respectively (Table **1**).

The selectivity index (SI) was calculated by comparing IC_{50} values in non-tumor cell lines (L-929 and PBMC) to the IC_{50} of the same compound in tumor cell lines. The SI of SSC185 was four (SI=4) for colorectal cancer cell lines HCT-116 and SW-620 and 2.8 for HL-60 cell line (SI=2.8). No selectivity was observed for the other cell lines. The selectivity index of doxorubicin, when comparing the IC_{50} value in PBMC with the tumor cells, ranged from 2 to 138 depending on the cell line tested.

3.3. Time and Concentration-Dependent Effect of SSC185 Against SW-620 and HCT-116 Cells

In view of the aggressiveness and high death rate of colorectal cancer [38], the discovery of new compounds with an apparently selective effect against colorectal cancer cells is interesting, and the study of the mechanism involved in the anticancer effect of these compounds is necessary. Thus, the selective cytotoxic effect of SSC185 against colorectal cancer cells presents opportunities for further study of the mechanism of cell death induced by this molecule.

The time- and concentration-dependent antitumor effect of SSC185 on HCT-116 and SW-620 cell lines was evaluated. It was observed that SSC185 showed no cytotoxic effect against HCT-116 (IC_{50}>52 μM) after 24 h of incubation but was able to inhibit cell proliferation of SW-620, with an IC_{50} value of 28.35 μM after the same incubation period. After 48 h of incubation, SSC185 showed IC_{50} values of 18.10 and 10.31 μM for HCT-116 and SW-620 cell lines, respectively (Table **2**). This indicates that SSC185 may have a distinct cytotoxic profile depending on the cell context and may also distinguish the mechanism of cell death.

Because SSC185 had an antitumor effect against the human metastatic colorectal cancer cell line (SW-620) with only 24 h of incubation, these cells were chosen to continue studies of the possible mechanism involved in the antitumor effect of this compound *in vitro*.

The SSC185 tumor inhibition profile in SW-620 cells was also assessed by real-time cell growth monitoring using the xCELLigence System (Fig. **5A**). Normalization of cell index values based on the negative control value for each incubation period analyzed allowed the percentage of inhibition of cell growth to be estimated. SSC185 (15 μM) was able to inhibit 37%, 53% and 67% of SW-620 cell growth after 24, 48 and 72 h incubation, respectively, while 10 μM SSC185 inhibited 13% of cell growth only after 72 h of incubation. Doxorubicin (0.5 μM) inhibited 32% and 69% of cell growth after 48 and 72 h of incubation, respectively (Fig. **5B**). These results show a time-dependent profile for the cytotoxic effect of SSC185 and are consistent with the results of the MTT assay, in which cell proliferation was also affected in a time-dependent manner.

3.4. Induction of Cell Death by SSC185 in SW-620 Cells

Many flavonoids are associated with colorectal cancer control and prevention, affecting carcinogenesis through different targets,

Table 1. Cytotoxicity of SSC185 against tumor and non-tumor cell lines. IC_{50} values obtained by MTT assay after 72 h of incubation. Data are presented as IC_{50} values and 95% confidence interval.

Cell Lines		IC_{50} (μM) 95% Confidence Interval	
		SSC185	Doxorubicin
Tumor	PC-3	29.52 (26.82-32.49)	0.76 (0.59-0.93)
	HCT-116	5.59 (5.22-6.01)	0.21 (0.16-0.29)
	SF-295	26.88 (27.91-33.69)	0.41 (0.21-0.47)
	NCI-H460	24.00 (20.27-28.41)	0.15 (0.13-0.18)
	SW-620	6.27 (5.84-6.74)	0.06 (0.04-0.10)
	HEP-G2	22.05 (18.79-25.87)	0.33 (0.29-0.37)
	MCF-7	19.76 (18.09-21.58)	0.15 (0.12-0.19)
	HL-60	8.46 (7.69-9.30)	0.02 (0.01-0.02)
Non-tumor	L-929	24.10 (21.40-27.14)	1.72 (1.58-1.87)
	PBMC	22.54 (20.59-24.66)	2.76 (2.30-3.31)

Table 2. Time- and concentration-dependent effect of SSC185 on HCT-116 and SW-620 cell viability determined by MTT assay. Data are presented as IC_{50} values and 95% confidence interval.

Cell Lines	IC_{50} (μM) 95% Confidence Interval		
	24 h	48 h	72 h
HCT-116	>52	18.10 (14.08-23.26)	5.59 (5.22-6.01)
SW-620	28.35 (25.16-31.93)	10.31 (9.28-11.46)	6.27 (5.84-6.74)

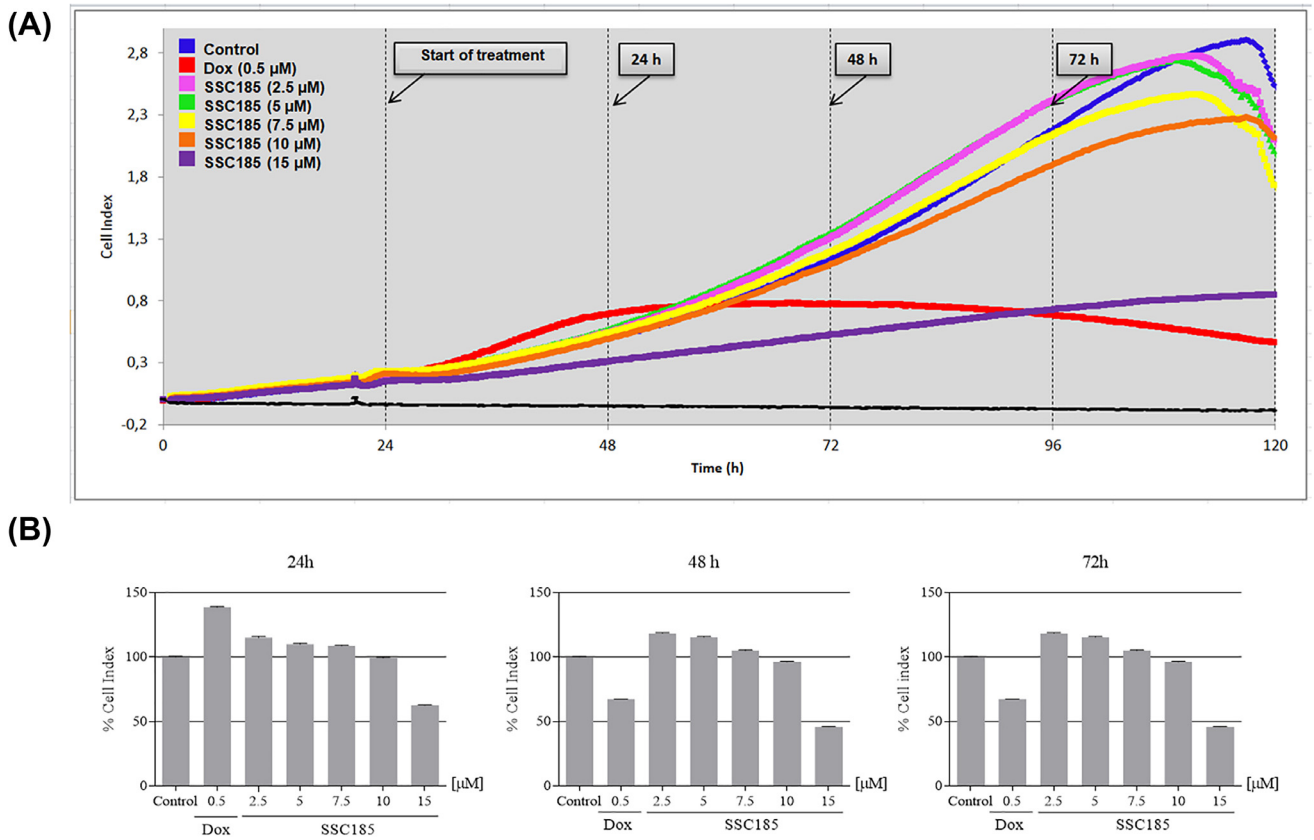

Fig. (5). Real-time monitoring of SW-620 cell growth inhibition during treatment with SSC185 by xCELLigence system. (**A**) Representative cell index of SW-620 cell growth after treatment with SSC185 (2.5, 5, 7.5, 10 and 15 μM) and Doxorubicin (0.5 μM) from a representative experiment. (**B**) Normalized cell index based on negative control (vehicle) for each incubation period analysed (24 h, 48 h and 72 h). (*A higher resolution / colour version of this figure is available in the electronic copy of the article*).

including cell cycle progression and apoptosis induction [39]. Chalcones, precursor molecules of flavonoids and isoflavonoids, have offered advantages as anticancer agents compared to other flavonoids due to their interaction with DNA and low risk of mutagenesis [40-42]. However, there are no studies that demonstrate the mechanism of cell death involved in the cytotoxic effect of sulfonamide chalcones.

To verify the mechanism of cell death involved in the cytotoxic effect of SSC185, morphological analysis of SSC185-treated SW-620 cells was performed using light microscopy and staining with the fast-panoptic kit. All tested concentrations of SSC185 induced the formation of apoptotic bodies in the membrane of some SW-620 cells, with the formation of blebs, and condensation and nuclear fragmentation, after 24 and 48 h of incubation. In addition to these changes, a change in the cytoplasmic membrane and the appearance of cell debris was observed (Fig. **6**). These characteristics are compatible with cell death of apoptotic and necrotic morphotypes.

Activation of intrinsic cell death programs or passive interruption of membrane integrity can result in cell death associated with an apoptotic or necrotic phenotype, respectively. Necrotic cell death has long been defined as a form of uncontrolled passive cell death. However, in addition to apoptosis, other intrinsic programs can lead to programmed necrotic cell death [43].

To confirm cell morphological changes observed by microscopy, and to evaluate the initial mechanism of cell death induced by SSC185, a flow cytometry membrane integrity analysis of SW-620 cells treated with SSC185 for 24 h was performed. SSC185 induced membrane damage and decreased the number of SW-620 cells at 10 and 15 μM concentrations after 24 h of incubation when compared

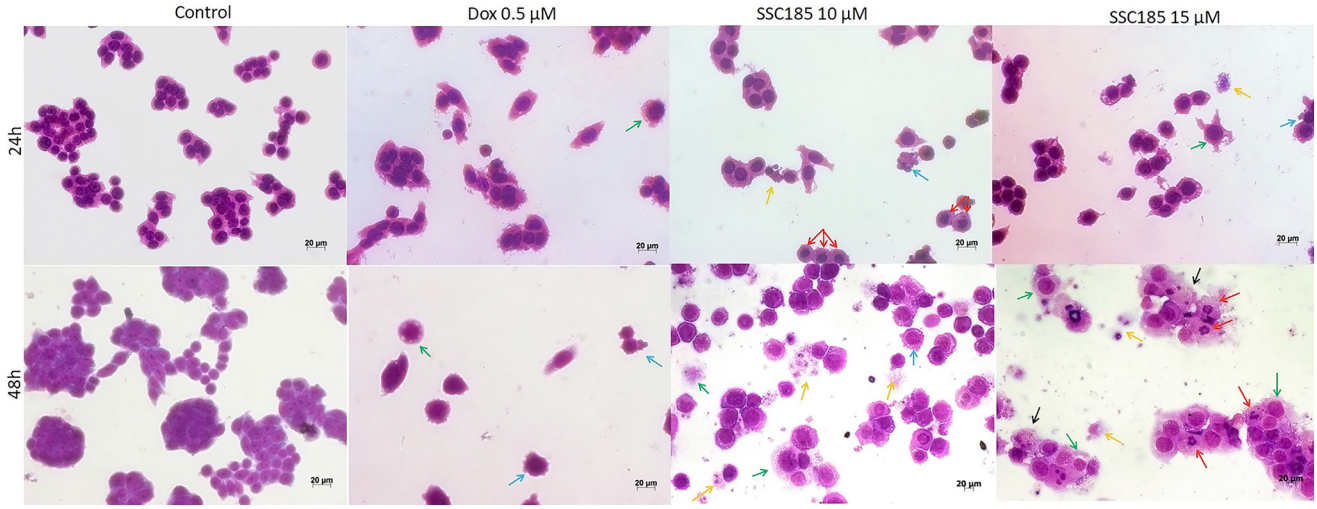

Fig. (6). SSC185 induced morphological changes in SW620 cells. Microscopic analysis of SW-620 cells fixed with methanol and counterstained with 0.1% xanthenes and 0.1% thiazines after 24 and 48 h of incubation. The cells were analysed by light microscopy (200×). Green arrows: cytoplasmic membrane changes; blue arrows: apoptotics bodies; yellow arrows: debris; red arrows: chromatin condensation and nuclear fragmentation; black arrows: extracellular release of cytoplasmic components. (*A higher resolution / colour version of this figure is available in the electronic copy of the article*).

to the negative control (**p* <0.05) (Fig. **7A** and **7B**), corroborating our findings with light microscopy.

Therefore, to verify the role of mitochondria in the cytotoxic effect of SSC185, the transmembrane potential of mitochondria (ΔΨm) was evaluated using flow cytometry by incorporation of Rhodamine 123 dye after 24 h of treatment. As observed in Fig. (**7C**), SSC185 induced significant (**p* <0.05) mitochondrial depolarization in 18.2% and 21.3% of SW-620 cells treated with 10 µM and 15 µM SSC185, respectively, when compared to the negative control (12.9%), after 24 h of incubation. Using fluorescence microscopy and staining with acridine orange and ethidium bromide, a differential cell count of viable, early apoptotic, late apoptotic or necrotic cells was performed. SSC185 induced a significant increase in necrotic cells with a consequent reduction in the number of viable cells after 24 h of incubation at 10 µM and 15 µM concentrations (Fig. **7D**).

Studies have shown the cytotoxic effect of various chalcone derivatives on several cancer cell lines [39, 44, 45]. In general, chalcones and chalcone derivatives induce cell death by apoptosis, resulting from a variety of cellular events, such as mitochondrial damage, modifications in oxidative metabolism with change in ATP content, and alterations in the expression of genes involved in the regulation of apoptosis [46-50]. However, research into the influence that added organic groups such as sulfonamide have on the mechanism of cell death induced by chalcones remains inconclusive [10-14].

Western blot assays were performed to evaluate the expression of cell death-related proteins in SSC185-treated SW-620 cells using concentrations of 10 µM and 15 µM after 24 h of treatment. Fig. (**7E**) shows that PARP cleavage was observed at both tested concentrations of SSC185. In addition, a reduction in pro-apoptotic Bax protein expression was observed at the 15 µM concentration, while the positive control, doxorubicin (0.5 µM), increased expression of this protein. Only cells treated with SSC185 (15 µM) did not demonstrate caspase 8 cleavage.

Programmed cell death is a complex network of interconnected signaling pathways that can result in several types of cell death, and death-regulating proteins can be involved in more than one type. While the RHIM (RIP homotypic interaction motif) domain of RIPK3 promotes apoptosis, the kinase activity of RIPK3 contributes to necroptosis [51]. Furthermore, hyperactivation of PARP may be related to the release of apoptosis-inducing factors as well as various types of necrosis, including necroptosis and response to DNA damage [52].

Necroptosis is a type of regulated necrosis that is increasingly being recognized by the scientific community as an important form of cell death [52]. This programmed necrotic cell death is characterized by the activation of controlled processes such as mitochondrial dysfunction, increased ROS generation by mitochondria, ATP depletion, calcium homeostasis failure, perinuclear organelle aggregation, PARP activation, lysosomal rupture, and plasma membrane permeabilization [53, 54]. Necroptosis critically depends on a sequential activation and phosphorylation of RIPK3 (receptor-interacting serine/threonine-protein kinase 3) and MLKL (mixed lineage kinase domain like pseudokinase) proteins and is induced by death receptors, interferons, toll-like receptors, and intracellular DNA and RNA sensors, among other mediators [55].

The biomarkers used to detect the activation of RIPK1, RIPK3, and MLKL in necroptosis include phosphorylated RIPK1/3 and MLKL. Apoptosis needs caspase activation, but necroptosis can induce tumor cell death when caspases are inhibited or defective [53, 54]. Thus, caspase-8 is a determining factor in apoptosis and necroptosis, required during the activation of apoptosis and suppressed in the activation of necroptosis. *In vitro* studies have demonstrated that inhibition of caspase-8 resulted in activation of RIPK3, a key player in necroptosis, as it phosphorylates MLKL [56, 57].

Given the relationship between caspase 8 cleavage inhibition and necroptosis activation, the influence of SSC185 on the expression of necroptosis-related proteins, MLKL and RIP, was evaluated. SSC185 reduced the expression of MLKL and RIP proteins at both concentrations tested when compared to the negative control, suggesting that one of the cell death mechanisms induced by this compound is necroptosis associated with caspase activation, depending on the SSC185 concentration tested (Fig. **7E**).

Additionally, SSC185 induced DNA fragmentation in SW-620 cells after 24 h of incubation, assessed by the percentage of cells in the sub-G1 phase using flow cytometry, probably related to oxidative stress (Fig. **8A**). Different types of cell death are often associated with mitochondrial dysfunction and the generation of reactive oxygen species (ROS). Therefore, to investigate the influence of ROS on the cytotoxic effect of SSC185, SW-620 cells were pre-

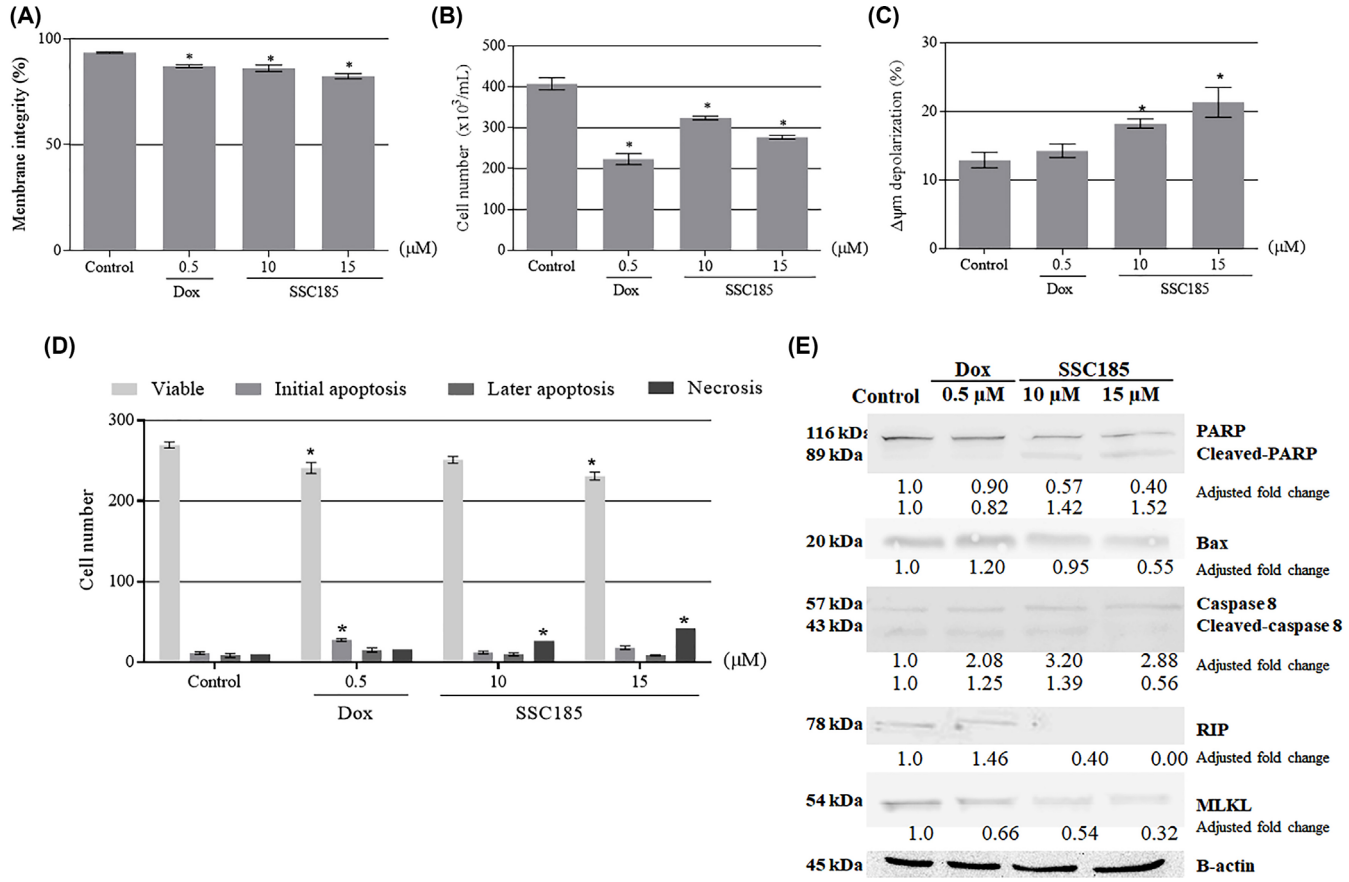

Fig. (7). SSC185 decreased membrane integrity of SW-620 cells, with mitochondrial depolarization and induction of necroptosis cell death. Effects of SSC185 on SW-620 (**A**) membrane integrity, (**B**) cell number, and (**C**) transmembrane mitochondrial potential, evaluated by flow cytometry after 24 h of incubation. (**D**) Mechanism of cell death involved in the cytotoxic effect of SSC185 in SW-620 cells after 24 h of incubation, determined by acridine orange and ethidium bromide staining by fluorescence microscopy. Data are presented as mean ± S.E.M. from three independent experiments performed in triplicate. (*) $p < 0.05$ compared to negative control by ANOVA followed by Tukey's test. Ten thousand events were analyzed in each experiment. (**E**) Representative Western blot analysis of cell death-related protein expression of SSC185-treated SW-620 cells after 24 h incubation. Doxorubicin (Dox - 0.5 μM) was used as a positive control. Adjusted fold change is shown.

treated for 2 h with N-acetyl-L-cysteine (NAC, 4 mM), an indirect way to assess oxidative stress. NAC is an antioxidant agent capable of sequestering formed ROS. These cells were then treated with serial concentrations of SSC185 for 48 h to determine the IC_{50}value by MTT assay. We can suggest that ROS participate in the cytotoxic effects of SSC185 since the IC_{50} value was higher when the SW-620 cells were pre-treated with NAC (IC_{50}= 30.30 μM). The positive control of the experiment, menadione (IC_{50}=16.98 μM), had a higher IC_{50} value when cells were pre-treated with NAC (IC_{50}= 27.36 μM) (Fig. **8B**). However, other assays are needed to confirm the participation of ROS in the cytotoxic effect of SSC185.

3.5. Induction of G2/M Cell Cycle Arrest by SSC185 in SW-620 Cells

There are no studies reporting the effect of sulfonamide chalcones on the cell cycle of tumor cells. However, some chalcones and their derivatives induce cell arrest in the G2/M phase of the cell cycle, cause nuclear fragmentation and condensation, and cell death by apoptosis by different mechanisms in different colorectal cancer cell lines [39, 41, 44, 45].

A group of proteins is activated and inactivated during the cell cycle. Cyclins are catalyzed and activated when bound to protein kinase-like enzymes called cyclin-dependent kinases (Cdk). This binding allows Cdks to perform the function of phosphorylating other proteins involved in the cell cycle. Each cyclin is specific for certain cell cycle periods, for example, Cyclin B is present at its highest levels during G2 and M phases [58].

DNA content flow cytometry analysis was performed to evaluate the effect of SSC185 on the cell cycle of SW-620. It was possible to observe a significant increase (*p <0.05) in the percentage of cells in the G2/M phase at both tested concentrations (10 μM and 15 μM) after 24 h of incubation. The positive control, doxorubicin (0.5 μM), induced G2/M phase cell cycle arrest (Fig. **9A**).

Key proteins involved in the G2/M phase were evaluated by Western blot. We observed an increased expression of cyclin B1 and pChk2 in cells incubated for 24 h with doxorubicin (0.5 μM) or SSC185 (10 μM), and a decrease in cyclin B1 expression when incubated with SSC185 (15 μM), compared to the negative control. An increase of pChk1 expression was observed only in cells treated with doxorubicin (0.5 μM) (Fig. **9B**).

Stress induction during the replication process and the cellular response to DNA damage in tumor cells activate ATR/Chk1 or ATM/Chk2, depending on the type of genotoxic stress. Their activation provides an anticancer barrier, often leading to the elimination of highly proliferative potential tumor cells by inducing cell death [59]. However, future studies can be carried out to assess whether SSC185 interferes with any DNA damage or repair pathway or even if it directly interacts with DNA.

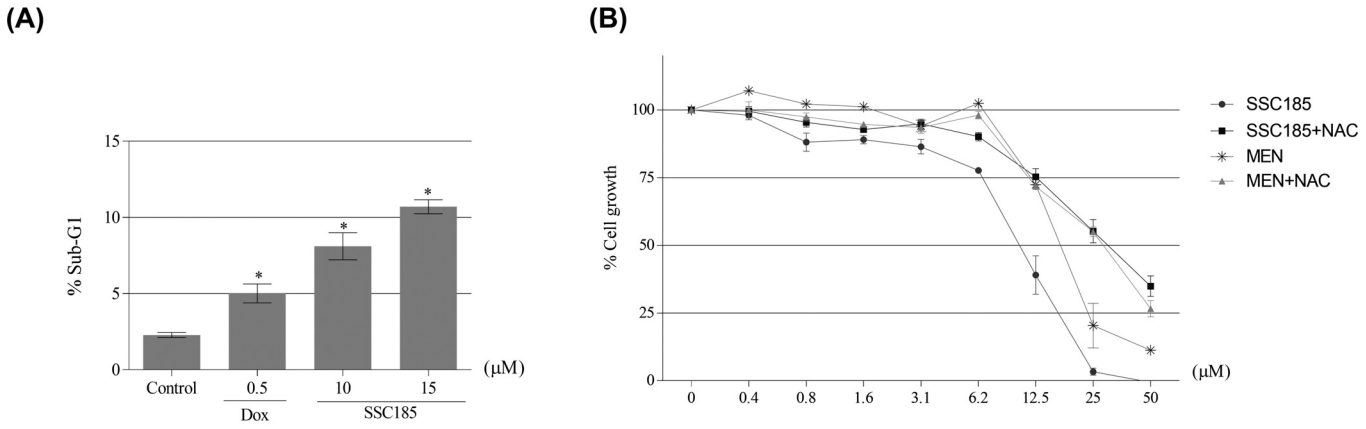

Cell lines	IC_{50} (μM) 95% confidence interval			
	SSC185	SSC185+NAC	MEN	MEN+NAC
SW-620	10.31 (9.28-11.46)	30.30 (27.30-33.63)	16.98 (15.35-18.79)	27.36 (24.49-30.56)

Fig. (8). SSC185 induced DNA fragmentation, probably related to oxidative stress induced by this compound. (**A**) DNA fragmentation represented by the percentage of Sub-G1 obtained by flow cytometry of SSC185-treated SW-620 cells after 24 h of incubation. Doxorubicin (Dox - 0.5 μM) was used as positive control. Data are presented as mean ± S.E.M. from three independent experiments performed in triplicate. (*) $p < 0.05$ compared to negative control by ANOVA followed by Tukey's test. (**B**) Cell growth of SW-620 cells pre-treated or not with N-acetyl-L-cysteine (NAC, 4 mM) for 2 h, and then treated with SSC185 for 48 h of incubation by MTT assay. Menadione (MEN) was used as a positive control. Data are presented as IC_{50} values and 95% confidence interval.

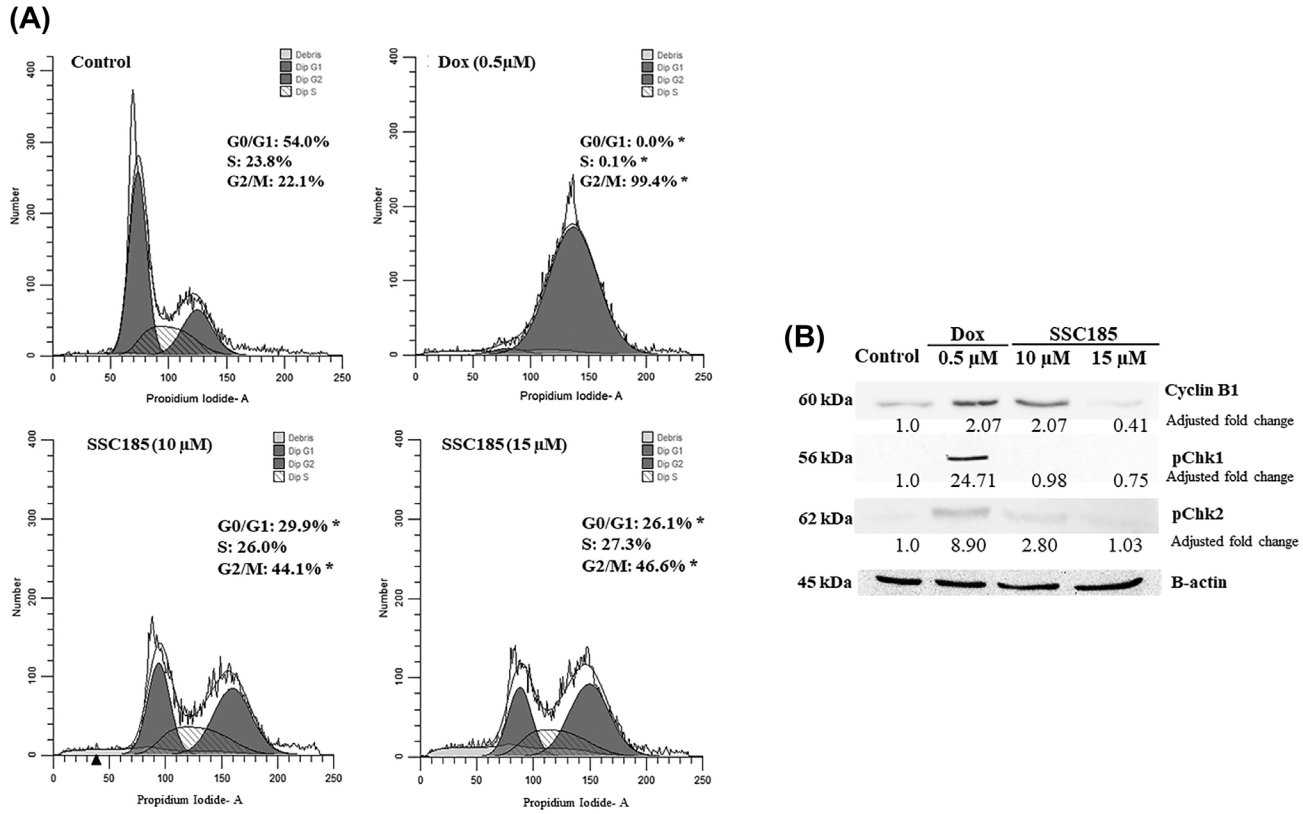

Fig. (9). SSC185 induced G2/M cell cycle arrest in SW-620 cells. (**A**) DNA content analysis of SSC185-treated SW-620 cells after 24 h of incubation by flow cytometry. Flow cytometry data are presented as mean ± S.E.M. values obtained from at least three experiments performed in triplicate. (*) $p < 0.05$ compared to negative control (Control) by ANOVA followed by Tukey's test. Ten thousand events were analysed by replicating in each experiment. (**B**) Representative Western blot analysis of cell cycle-related protein expression of SSC185-treated SW-620 cells after 24 h incubation. Doxorubicin (Dox - 0.5 μM) was used as positive control. Adjusted fold change is shown.

CONCLUSION

The mechanism of cell death induced by SSC185 may be related to G2/M cell cycle arrest, associated with the induction of mitochondrial depolarization and cell death occurring by apoptosis or necroptosis, depending on the concentration used. Further studies are needed to explain the higher activity of SSC185 in colorectal cancer cells.

LIST OF ABBREVIATIONS

SSC185	=	Synthetic Sulfonamide Chalcone 185
JKN3	=	Mitogen-activated Protein kinase 10
BSA	=	Bovine Serum Albumin
FTIR	=	Fourier-Transform Infrared Spectroscopy
NMR	=	Nuclear Magnetic Resonance
IC50	=	Half Maximal Inhibitory Concentration
PBMC	=	Peripheral Blood Mononuclear Cell
SI	=	Selectivity Index
ROS	=	Reactive Oxygen Species
NAC	=	N-Acetyl-L-Cysteine
Dox	=	Doxorubicin
MEN	=	Menadione
DMEM	=	Dulbecco' smodifiedeagle' sminimalessentialmedium
MTT	=	Tetrazolium 3-(4,5-dimethyl-2-thiazole)-2,5-diphenyl-bromide salt
DMSO	=	Dimethyl Sulfoxide
PBS	=	Phosphate Buffer Solution

ETHICS APPROVAL AND CONSENT TO PARTICIPATE

Human and murine cell lines were PC-3 (prostate), HCT-116 (colon), SF-295 (brain), NCI-H460 (lung), SW-620 (metastatic colon), HEP-G2 (liver), MCF-7 (breast), HL-60 (promyelocytic leukemia) and L-929 (fibroblast) non-tumor cell lines were provided by the National Cancer Institute (Bethesda, MD, USA).

The project was approved by the research ethics committee of Universidade Federal do Delta do Parnaíba, Campus Ministro Reis Velloso, under protocol number 4.844.208.

HUMAN AND ANIMAL RIGHTS

No animals/humans were used for studies that are the basis of this research.

CONSENT FOR PUBLICATION

Not applicable.

AVAILABILITY OF DATA AND MATERIALS

Not applicable.

FUNDING

This study has been funded by Coordenação de Aperfeiçoamento de Pessoal de Nível Superior (CAPES) and Conselho Nacional de Desenvolvimento Científico e Tecnológico (CNPq).

CONFLICT OF INTEREST

The authors declare no conflict of interest, financial or otherwise.

ACKNOWLEDGEMENTS

The authors thank Coordenação de Aperfeiçoamento de Pessoal de Nível Superior (CAPES) and Conselho Nacional de Desenvolvimento Científico e Tecnológico (CNPq) for the financial support.

SUPPLEMENTARY MATERIAL

All information related to the collection, treatment and refinement of crystal structures is presented in the Table S1 of the Supplementary Information.

H NMR spectra of μ- (2,5-dichloro-N-{4-[(3E)-4-(3-nitrophenyl)buta-1,3-dien-2-yl]phenyl}benzene sulfonamide are in Supplementary Material.

Supplementary material is available on the publisher's website along with the published article.

REFERENCES

[1] American Cancer Society. **2020**. Available from: https://www.cancer.org/treatment/treatments-and-sideeffects/treatment-types.html (Accessed Jan 20, 2021).

[2] Bortner, C.D.; Cidlowski, J.A. Ion channels and apoptosis in cancer. *Philos. Trans. R. Soc. Lond. B Biol. Sci.,* **2014**, *369*(1638), 20130104. http://dx.doi.org/10.1098/rstb.2013.0104 PMID: 24493752

[3] Fouad, Y.A.; Aanei, C. Revisiting the hallmarks of cancer. *Am. J. Cancer Res.,* **2017**, *7*(5), 1016-1036. PMID: 28560055

[4] Hanahan, D.; Weinberg, R.A. Hallmarks of cancer: The next generation. *Cell,* **2011**, *144*(5), 646-674. http://dx.doi.org/10.1016/j.cell.2011.02.013 PMID: 21376230

[5] Ouyang, Y.; Li, J.; Chen, X.; Fu, X.; Sun, S.; Wu, Q. Chalcone derivatives: Role in anticancer therapy. *Biomolecules,* **2021**, *11*(6), 894. http://dx.doi.org/10.3390/biom11060894 PMID: 34208562

[6] Pesaran Seiied Bonakdar, A.; Vafaei, F.; Farokhpour, M.; Nasr Esfahani, M.H.; Massah, A.R. Synthesis and anticancer activity assay of novel chalcone-sulfonamide derivatives. *Iran. J. Pharm. Res.,* **2017**, *16*(2), 565-568. PMID: 28979310

[7] Bahekar, S.P.; Hande, S.V.; Agrawal, N.R.; Chandak, H.S.; Bhoj, P.S.; Goswami, K.; Reddy, M.V.R. Sulfonamide chalcones: Synthesis and *in vitro* exploration for therapeutic potential against *Brugia malayi. Eur. J. Med. Chem.,* **2016**, *124*, 262-269. http://dx.doi.org/10.1016/j.ejmech.2016.08.042 PMID: 27592395

[8] Domínguez, J.N.; León, C.; Rodrigues, J.; Gamboa de Domínguez, N.; Gut, J.; Rosenthal, P.J. Synthesis and antimalarial activity of sulfonamide chalcone derivatives. *Farmaco,* **2005**, *60*(4), 307-311. http://dx.doi.org/10.1016/j.farmac.2005.01.005 PMID: 15848205

[9] Tang, Y.L.; Li, Y.K.; Li, M.X.; Gao, H.; Yang, X.B.; Mao, Z.W. Synthesis of new piperazine substituted chalcone sulphonamides as antibacterial agents. *Curr. Org. Synth.,* **2020**, *17*(2), 136-143. http://dx.doi.org/10.2174/1570179417666191227115207 PMID: 32418516

[10] Castaño, L.F.; Cuartas, V.; Bernal, A.; Insuasty, A.; Guzman, J.; Vidal, O.; Rubio, V.; Puerto, G.; Lukáč, P.; Vimberg, V.; Balíková-Novtoná, G.; Vannucci, L.; Janata, J.; Quiroga, J.; Abonia, R.; Nogueras, M.; Cobo, J.; Insuasty, B. New chalcone-sulfonamide hybrids exhibiting anticancer and antituberculosis activity. *Eur. J. Med. Chem.,* **2019**, *176*, 50-60. http://dx.doi.org/10.1016/j.ejmech.2019.05.013 PMID: 31096118

[11] de Castro, M.R.C.; Aragão, A.Q.; da Silva, C.C.; Perez, C.N.; Queiroz, D.P.K.; Queiroz Júnior, L.H.K.; Barreto, S.; de Moraes, M.O.; Martins, F.T. Conformational variability in sulfonamide chalcone hybrids: Crystal structure and cytotoxicity. *J. Braz. Chem. Soc.,* **2016**, *27*(5), 884-898. http://dx.doi.org/10.5935/0103-5053.20150341

[12] Custodio, J.M.F.; Michelini, L.J.; de Castro, M.R.C.; Vaz, W.F.; Neves, B.J.; Cravo, P.V.L.; Barreto, F.S.; Moraes Filho, M.O.; Perez, C.N.; Napolitano, H.B. Structural insights into a novel anticancer sulfonamide chalcone. *NJC,* **2018**, *5*, 1-9. http://dx.doi.org/10.1039/C7NJ03523C

[13] D'Oliveira, G.D.C.; Moura, A.F.; Moraes, M.O.; Perez, C.N.; Lião, L.M. Synthesis, characterization and evaluation of *in vitro* antitumor activities of novel chalcone-quinolinone hybrid compounds. *J. Braz. Chem. Soc.,* **2018**, *29*(11), 2308-2325. http://dx.doi.org/10.21577/0103-5053.20180108

[14] Pesaran Seiied Bonakdar, A.; Vafaei, F.; Farokhpour, M.; Nasr Esfahani, M.H.; Massah, A.R. Synthesis and anticancer activity assay of novel chalcone sulfonamide derivatives. *Iran. J. Pharm. Res.,* **2017**, *16*(2), 565-568. PMID: 28979310

[15] Seo, W.D.; Kim, J.H.; Kang, J.E.; Ryu, H.W.; Curtis-Long, M.J.; Lee, H.S.; Yang, M.S.; Park, K.H. Sulfonamide chalcone as a new class of alpha-glucosidase inhibitors. *Bioorg. Med. Chem. Lett.,* **2005**, *15*(24), 5514-5516. http://dx.doi.org/10.1016/j.bmcl.2005.08.087 PMID: 16202584

[16] Kang, J.E.; Cho, J.K.; Curtis-Long, M.J.; Ryu, H.W.; Kim, J.H.; Kim, H.J.; Yuk, H.J.; Kim, D.W.; Park, K.H. Inhibitory evaluation of sulfonamide chalcones on β-secretase and acylcholinesterase. *Molecules,* **2012**, *18*(1), 140-153. http://dx.doi.org/10.3390/molecules18010140 PMID: 23344193

[17] Arslan, T.; Türkoğlu, E.A.; Şentürk, M.; Supuran, C.T. Synthesis and carbonic anhydrase inhibitory properties of novel chalcone substituted benzenesulfonamides. *Bioorg. Med. Chem. Lett.,* **2016**, *26*(24), 5867-5870. http://dx.doi.org/10.1016/j.bmcl.2016.11.017 PMID: 27884694

[18] Peerzada, M.N.; Khan, P.; Ahmad, K.; Hassan, M.I.; Azam, A. Synthesis, characterization and biological evaluation of tertiary sulfonamide derivatives of pyridyl-indole based heteroaryl chalcone as potential carbonic anhydrase IX inhibitors and anticancer agents. *Eur. J. Med. Chem.,* **2018**, *155*, 13-23. http://dx.doi.org/10.1016/j.ejmech.2018.05.034 PMID: 29852328

[19] Singh, P.; Swain, B.; Thacker, P.S.; Sigalapalli, D.K.; Purnachander Yadav, P.; Angeli, A.; Supuran, C.T.; Arifuddin, M. Synthesis and carbonic anhydrase inhibition studies of sulfonamide based indole-1,2,3-triazole chalcone hybrids. *Bioorg. Chem.,* **2020**, *99*, 103839. http://dx.doi.org/10.1016/j.bioorg.2020.103839 PMID: 32289586

[20] Ejaz, S.A.; Saeed, A.; Siddique, M.N.; Nisa, Z.U.; Khan, S.; Lecka, J.; Sévigny, J.; Iqbal, J. Synthesis, characterization and biological evaluation of novel chalcone sulfonamide hybrids as potent intestinal alkaline phosphatase inhibitors. *Bioorg. Chem.,* **2017**, *70*, 229-236. http://dx.doi.org/10.1016/j.bioorg.2017.01.003 PMID: 28110961

[21] Custodio, J.M.F.; Moura, A.F.; Moraes, M.O.; Perez, C.N.; Napolitano, H.B. On the *in silico* and *in vitro* anticancer activity of sulfonamide chalcones: Potential JNKK3 inhibitors. *New J. Chem.,* **2020**, *44*(8), 3294-3309. http://dx.doi.org/10.1039/C9NJ05612B

[22] Lee, B.; Kang, W.; Shon, J.; Park, K.H.; Song, K-S.; Liu, K-H. Potential of 4′-(p-toluene sulfonamide)-4-hydroxychalcone to inhibit the human cytochrome p450 2j2 isoform. *Appl. Biol. Chem,* **2014**, *57*(1), 31-34.

[23] Lee, S-A.; Lee, M-S.; Ryu, H.W.; Kwak, T.K.; Kim, H.; Kang, M.; Jung, O.; Kim, H.J.; Park, K.H.; Lee, J.W. Differential inhibition of transmembrane 4 L six family member 5 (TM4SF5)-mediated tumorigenesis by TSAHC and sorafenib. *Cancer Biol. Ther.,* **2011**, *11*(3), 330-336. http://dx.doi.org/10.4161/cbt.11.3.14099 PMID: 21099346

[24] Ghorab, M.M.; Ragab, F.A.; Heiba, H.I.; El-Gazzar, M.G.; Zahran, S.S. Synthesis, anticancer and radiosensitizing evaluation of some novel sulfonamide derivatives. *Eur. J. Med. Chem.,* **2015**, *92*, 682-692. http://dx.doi.org/10.1016/j.ejmech.2015.01.036 PMID: 25618015

[25] APEX2. *Bruker AXS Inc*; Madison, Wisconsin, USA, **2009**.

[26] Burla, M.C.; Caliandro, R.; Camalli, M.; Carrozzini, B.; Cascarano, G.L.; De Caro, L.; Giacovazzo, C.; Polidori, G.; Spagna, R. SIR2004: An improved tool for crystal structure determination and refinement. *J. Appl. Cryst.,* **2005**, *38*, 381-388. http://dx.doi.org/10.1107/S002188980403225X

[27] Sheldrick, G.M. Crystal structure refinement with SHELXL. *ActaCrystallogr. Sect. C,* **2015**, *71*(Pt 1), 3-8. http://dx.doi.org/10.1107/S2053229614024218 PMID: 25567568

[28] Macrae, C.F.; Bruno, I.J.; Chisholm, J.A.; Edgington, P.R.; McCabe, P.; Pidcock, E.; Rodriguez-Monge, L.; Taylor, R.; van de Streek, J.; Wood, P.A. Mercury CSD 2.0 – new features for the visualization and investigation of crystal structures. *J. Appl. Cryst.,* **2008**, *41*, 466-470. http://dx.doi.org/10.1107/S0021889807067908

[29] Farrugia, L.J. WinGX and ORTEP for Windows: An update. *J. Appl. Cryst.,* **2012**, *45*, 849-854. http://dx.doi.org/10.1107/S0021889812029111

[30] Moura, A.F.; Lima, K.S.B.; Sousa, T.S.; Marinho-Filho, J.D.B.; Pessoa, C.; Silveira, E.R.; Pessoa, O.D.L.; Costa-Lotufo, L.V.; Moraes, M.O.; Araújo, A.J. *In vitro* antitumor effect of a lignan isolated from *Combretum* fruticosum, trachelogenin, in HCT-116 human colon cancer cells. *Toxicol. In Vitro,* **2018**, *47*, 129-136. http://dx.doi.org/10.1016/j.tiv.2017.11.014 PMID: 29174024

[31] Mosmann, T. Rapid colorimetric assay for cellular growth and survival: Application to proliferation and cytotoxicity assays. *J. Immunol. Methods,* **1983**, *65*(1-2), 55-63. http://dx.doi.org/10.1016/0022-1759(83)90303-4 PMID: 6606682

[32] Darzynkiewicz, Z.; Bruno, S.; Del Bino, G.; Gorczyca, W.; Hotz, M.A.; Lassota, P.; Traganos, F. Features of apoptotic cells measured by flow cytometry. *Cytometry,* **1992**, *13*(8), 795-808. http://dx.doi.org/10.1002/cyto.990130802 PMID: 1333943

[33] Cury-Boaventura, M.F.; Pompéia, C.; Curi, R. Comparative toxicity of oleic acid and linoleic acid on Jurkat cells. *Clin. Nutr.,* **2004**, *23*(4), 721-732. http://dx.doi.org/10.1016/j.clnu.2003.12.004 PMID: 15297111

[34] Schneider, C.A.; Rasband, W.S.; Eliceiri, K.W. NIH Image to ImageJ: 25 years of image analysis. *Nat. Methods,* **2012**, *9*(7), 671-675. http://dx.doi.org/10.1038/nmeth.2089 PMID: 22930834

[35] De Castro, M.R.C.; Naves, R.F.; Bernardes, A.; Silva, C.C.; Perez, C.N.; Moura, A.F.; Moraes, M.O.; Martins, F.T. Tandem chalcone-sulfonamide hybridization, cyclization and further Claisen–Schmidt condensation: Tuning molecular diversity through reaction time and order and catalyst. *Arab. J. Chem.,* **2020**, *13*(1), 1345-1354. http://dx.doi.org/10.1016/j.arabjc.2017.11.005

[36] Custodio, J.M.F.; Vaz, W.F.; de Castro, M.R.C.; Bernardes, A.; Naves, L.F.N.; Moura, A.F.; Moraes, M.O.; Silva, C.C.; Martins, F.T.; Perez, C.N.; Napolitano, H.B. Solvent-driven structural adaptation in a novel anticancer sulfonamide chalcone. *J. Mol. Struct.,* **2019**, *1175*, 389-397. http://dx.doi.org/10.1016/j.molstruc.2018.07.059

[37] Michelini, L.J.; Castro, M.R.C.; Custodio, J.M.F.; Naves, L.F.N.; Vaz, W.F.; Lobón, G.S.; Martins, F.T.; Perez, C.N.; Napolitano, H.B. A novel potential anticancer chalcone: Synthesis, crystal structure and cytotoxic assay. *J. Mol. Struct.,* **2018**, *1168*, 309-315. http://dx.doi.org/10.1016/j.molstruc.2018.05.010

[38] WHO. World Health Organization **2018**. Available from: https://www.who.int/en/news-room/fact-sheets/detail/cancer/ (Accessed Apr 2, 2020).

[39] Kello, M.; Drutovic, D.; Pilatova, M.B.; Tischlerova, V.; Perjesi, P.; Mojzis, J. Chalcone derivatives cause accumulation of colon cancer cells in the G2/M phase and induce apoptosis. *Life Sci.,* **2016**, *150*, 32-38. http://dx.doi.org/10.1016/j.lfs.2016.02.073 PMID: 26916824

[40] Amado, N.G.; Predes, D.; Moreno, M.M.; Carvalho, I.O.; Mendes, F.A.; Abreu, J.G. Flavonoids and Wnt/β-catenin signaling: Potential role in colorectal cancer therapies. *Int. J. Mol. Sci.,* **2014**, *15*(7), 12094-12106. http://dx.doi.org/10.3390/ijms150712094 PMID: 25007066

[41] Fonseca, B.F.; Predes, D.; Cerqueira, D.M.; Reis, A.H.; Amado, N.G.; Cayres, M.C.; Kuster, R.M.; Oliveira, F.L.; Mendes, F.A.; Abreu, J.G. Derricin and derricidin inhibit Wnt/β-catenin signaling and suppress colon cancer cell growth *in vitro*. *PLoS One,* **2015**, *10*(3), e0120919. http://dx.doi.org/10.1371/journal.pone.0120919 PMID: 25775405

[42] Pericleous, M.; Mandair, D.; Caplin, M.E. Diet and supplements and their impact on colorectal cancer. *J. Gastrointest. Oncol.,* **2013**, *4*(4), 409-423. http://dx.doi.org/10.3978/j.issn.2078-6891.2013.003 PMID: 24294513

[43] Zhang, Y.; Chen, X.; Gueydan, C.; Han, J. Plasma membrane changes during programmed cell deaths. *Cell Res.,* **2018**, *28*(1), 9-21.

http://dx.doi.org/10.1038/cr.2017.133 PMID: 29076500

[44] Drutovic, D.; Chripkova, M.; Pilatova, M.; Kruzliak, P.; Perjesi, P.; Sarissky, M.; Lupi, M.; Damia, G.; Broggini, M.; Mojzis, J. Benzylidenetetralones, cyclic chalcone analogues, induce cell cycle arrest and apoptosis in HCT116 colorectal cancer cells. *Tumour Biol.,* **2014**, *35*(10), 9967-9975. http://dx.doi.org/10.1007/s13277-014-2289-y PMID: 25008568

[45] Kim, Y.J.; Kang, K.S.; Choi, K.C.; Ko, H. Cardamonin induces autophagy and an antiproliferative effect through JNK activation in human colorectal carcinoma HCT116 cells. *Bioorg. Med. Chem. Lett.,* **2015**, *25*(12), 2559-2564. http://dx.doi.org/10.1016/j.bmcl.2015.04.054 PMID: 25959811

[46] de Vasconcelos, A.; Campos, V.F.; Nedel, F.; Seixas, F.K.; Dellagostin, O.A.; Smith, K.R.; de Pereira, C.M.; Stefanello, F.M.; Collares, T.; Barschak, A.G. Cytotoxic and apoptotic effects of chalcone derivatives of 2-acetyl thiophene on human colon adenocarcinoma cells. *Cell Biochem. Funct.,* **2013**, *31*(4), 289-297. http://dx.doi.org/10.1002/cbf.2897 PMID: 22987398

[47] Dong, N.; Liu, X.; Zhao, T.; Wang, L.; Li, H.; Zhang, S.; Li, X.; Bai, X.; Zhang, Y.; Yang, B. Apoptosis-inducing effects and growth inhibitory of a novel chalcone, in human hepatic cancer cells and lung cancer cells. *Biomed. Pharmacother.,* **2018**, *105*, 195-203. http://dx.doi.org/10.1016/j.biopha.2018.05.126 PMID: 29857299

[48] Dos Santos, M.B.; Bertholin Anselmo, D.; de Oliveira, J.G.; Jardim-Perassi, B.V.; Alves Monteiro, D.; Silva, G.; Gomes, E.; Lucia Fachin, A.; Marins, M.; de Campos Zuccari, D.A.P.; Octavio Regasini, L. Antiproliferative activity and p53 upregulation effects of chalcones on human breast cancer cells. *J. Enzyme Inhib. Med. Chem.,* **2019**, *34*(1), 1093-1099. http://dx.doi.org/10.1080/14756366.2019.1615485 PMID: 31117836

[49] Mielcke, T.R.; Muradás, T.C.; Filippi-Chiela, E.C.; Amaral, M.E.A.; Kist, L.W.; Bogo, M.R.; Mascarello, A.; Neuenfeldt, P.D.; Nunes, R.J.; Campos, M.M. Mechanisms underlying the antiproliferative effects of a series of quinoxaline-derived chalcones. *Sci. Rep.,* **2017**, *7*(1), 15850. http://dx.doi.org/10.1038/s41598-017-16199-3 PMID: 29158524

[50] Zhang, S.; Li, T.; Zhang, L.; Wang, X.; Dong, H.; Li, L.; Fu, D.; Li, Y.; Zi, X.; Liu, H.M.; Zhang, Y.; Xu, H.; Jin, C.Y. A novel chalcone derivative S17 induces apoptosis through ROS dependent DR5 up-regulation in gastric cancer cells. *Sci. Rep.,* **2017**, *7*(1), 9873. http://dx.doi.org/10.1038/s41598-017-10400-3 PMID: 28852176

[51] Pasparakis, M.; Vandenabeele, P. Necroptosis and its role in inflammation. *Nature,* **2015**, *517*(7534), 311-320. http://dx.doi.org/10.1038/nature14191 PMID: 25592536

[52] Galluzzi, L.; Vitale, I.; Aaronson, S.A.; Abrams, J.M.; Adam, D.; Agostinis, P.; Alnemri, E.S.; Altucci, L.; Amelio, I.; Andrews, D.W.; Annicchiarico-Petruzzelli, M.; Antonov, A.V.; Arama, E.; Baehrecke, E.H.; Barlev, N.A.; Bazan, N.G.; Bernassola, F.; Bertrand, M.J.M.; Bianchi, K.; Blagosklonny, M.V.; Blomgren, K.; Borner, C.; Boya, P.; Brenner, C.; Campanella, M.; Candi, E.; Carmona-Gutierrez, D.; Cecconi, F.; Chan, F.K.; Chandel, N.S.; Cheng, E.H.; Chipuk, J.E.; Cidlowski, J.A.; Ciechanover, A.; Cohen, G.M.; Conrad, M.; Cubillos-Ruiz, J.R.; Czabotar, P.E.; D'Angiolella, V.; Dawson, T.M.; Dawson, V.L.; De Laurenzi, V.; De Maria, R.; Debatin, K.M.; DeBerardinis, R.J.; Deshmukh, M.; Di Daniele, N.; Di Virgilio, F.; Dixit, V.M.; Dixon, S.J.; Duckett, C.S.; Dynlacht, B.D.; El-Deiry, W.S.; Elrod, J.W.; Fimia, G.M.; Fulda, S.; García-Sáez, A.J.; Garg, A.D.; Garrido, C.; Gavathiotis, E.; Golstein, P.; Gottlieb, E.; Green, D.R.; Greene, L.A.; Gronemeyer, H.; Gross, A.; Hajnoczky, G.; Hardwick, J.M.; Harris, I.S.; Hengartner, M.O.; Hetz, C.; Ichijo, H.; Jäättelä, M.; Joseph, B.; Jost, P.J.; Juin, P.P.; Kaiser, W.J.; Karin, M.; Kaufmann, T.; Kepp, O.; Kimchi, A.; Kitsis, R.N.; Klionsky, D.J.; Knight, R.A.; Kumar, S.; Lee, S.W.; Lemasters, J.J.; Levine, B.; Linkermann, A.; Lipton, S.A.; Lockshin, R.A.; López-Otín, C.; Lowe, S.W.; Luedde, T.; Lugli, E.; MacFarlane, M.; Madeo, F.; Malewicz, M.; Malorni, W.; Manic, G.; Marine, J.C.; Martin, S.J.; Martinou, J.C.; Medema, J.P.; Mehlen, P.; Meier, P.; Melino, S.; Miao, E.A.; Molkentin, J.D.; Moll, U.M.; Muñoz-Pinedo, C.; Nagata, S.; Nuñez, G.; Oberst, A.; Oren, M.; Overholtzer, M.; Pagano, M.; Panaretakis, T.; Pasparakis, M.; Penninger, J.M.; Pereira, D.M.; Pervaiz, S.; Peter, M.E.; Piacentini, M.; Pinton, P.; Prehn, J.H.M.; Puthalakath, H.; Rabinovich, G.A.; Rehm, M.; Rizzuto, R.; Rodrigues, C.M.P.; Rubinsztein, D.C.; Rudel, T.; Ryan, K.M.; Sayan, E.; Scorrano, L.; Shao, F.; Shi, Y.; Silke, J.; Simon, H.U.; Sistigu, A.; Stockwell, B.R.; Strasser, A.; Szabadkai, G.; Tait, S.W.G.; Tang, D.; Tavernarakis, N.; Thorburn, A.; Tsujimoto, Y.; Turk, B.; Vanden Berghe, T.; Vandenabeele, P.; Vander Heiden, M.G.; Villunger, A.; Virgin, H.W.; Vousden, K.H.; Vucic, D.; Wagner, E.F.; Walczak, H.; Wallach, D.; Wang, Y.; Wells, J.A.; Wood, W.; Yuan, J.; Zakeri, Z.; Zhivotovsky, B.; Zitvogel, L.; Melino, G.; Kroemer, G. Molecular mechanisms of cell death: Recommendations of the nomenclature committee on cell death 2018. *Cell Death Differ.,* **2018**, *25*(3), 486-541. http://dx.doi.org/10.1038/s41418-017-0012-4 PMID: 29362479

[53] Gong, Y.; Fan, Z.; Luo, G.; Yang, C.; Huang, Q.; Fan, K.; Cheng, H.; Jin, K.; Ni, Q.; Yu, X.; Liu, C. The role of necroptosis in cancer biology and therapy. *Mol. Cancer,* **2019**, *18*(1), 100. http://dx.doi.org/10.1186/s12943-019-1029-8 PMID: 31122251

[54] Su, Z.; Yang, Z.; Xie, L.; DeWitt, J.P.; Chen, Y. Cancer therapy in the necroptosis era. *Cell Death Differ.,* **2016**, *23*(5), 748-756. http://dx.doi.org/10.1038/cdd.2016.8 PMID: 26915291

[55] Cao, M.; Chen, F.; Xie, N.; Cao, M.Y.; Chen, P.; Lou, Q.; Zhao, Y.; He, C.; Zhang, S.; Song, X.; Sun, Y.; Zhu, W.; Mou, L.; Luan, S.; Gao, H. c-Jun N-terminal kinases differentially regulate TNF- and TLRs-mediated necroptosis through their kinase-dependent and -independent activities. *Cell Death Dis.,* **2018**, *9*(12), 1140. http://dx.doi.org/10.1038/s41419-018-1189-2 PMID: 30442927

[56] Holler, N.; Zaru, R.; Micheau, O.; Thome, M.; Attinger, A.; Valitutti, S.; Bodmer, J.L.; Schneider, P.; Seed, B.; Tschopp, J. Fas triggers an alternative, caspase-8-independent cell death pathway using the kinase RIP as effector molecule. *Nat. Immunol.,* **2000**, *1*(6), 489-495. http://dx.doi.org/10.1038/82732 PMID: 11101870

[57] Kaczmarek, A.; Vandenabeele, P.; Krysko, D.V. Necroptosis: the release of damage-associated molecular patterns and its physiological relevance. *Immunity,* **2013**, *38*(2), 209-223. http://dx.doi.org/10.1016/j.immuni.2013.02.003 PMID: 23438821

[58] Aleem, E.; Arceci, R.J. Targeting cell cycle regulators in hematologic malignancies. *Front. Cell Dev. Biol.,* **2015**, *3*(16), 16. http://dx.doi.org/10.3389/fcell.2015.00016 PMID: 25914884

[59] Sherr, C.J.; Bartek, J. Cell cycle – Targeted cancer therapies. *Annu. Rev. Cancer Biol.,* **2017**, *1*, 41-57. http://dx.doi.org/10.1146/annurev-cancerbio-040716-075628